SICE Annual Conference 2007
Sept. 17-20, 2007, Kagawa University, Japan

Gravity-Based 3D Shape Measuring Sheet

Takayuki Hoshi[1] and Hiroyuki Shinoda[1]

[1] Department of Information Physics and Computing, The University of Tokyo, Tokyo, Japan
(Tel : +81-3-5841-6927; E-mail: {star, shino}@alab.t.u-tokyo.ac.jp)

Abstract: In this paper, we introduce a novel sensing device named "3-dimensional capture sheet (3DCS)." The cloth-like sheet measures its own 3D configuration. It consists of a lattice structure inside of the sheet, and each link of the structure has a triaxial accelerometer. Though the roll and pitch angles of the link are calculated from the gravity vector measured with the accelerometer, the yaw angle is not determined by the gravity vector alone. Two approaches are proposed to obtain the angle; one approach utilizes constraints originating from the lattice structure, and the other takes the Earth's magnetic field as additional information. The whole shape of the sheet is reconstructed by combining the postures of all the links.

Keywords: Sensor network, 3-dimensional configuration, Flexible sensing device, Gravity, Geomagnetic field

1. INTRODUCTION

Providing intelligent functions for fabrics has often been reported in the field of wearable computing [1]-[3]. In early studies, in order to realize functionality, several middle-sized sensors were attached on fabrics or clothes. Recently, it is getting easier to embed a large number of down-sized and low-cost sensors in elastic cloth-like materials, due to the recent advances in CMOS-MEMS [4] and the new sensor networking technology [5].

Motivated by that trend, we propose a novel cloth-like device that measures its own 3D shape and motion by utilizing a large number of sensors distributed on it. The device is named "3-dimensional capture sheet (3DCS)." One of the conventional methods for observing the cloth motion is to utilize optical methods like the optical 3D digitizers [6]. However, such methods are weak against the self-occluding situation. In addition, optical methods require external equipments such as cameras and light sources, which can be drawbacks in some applications. The 3DCS does not suffer from the self-occlusion problem and requires no external equipments.

The 3DCS has several potential applications. First, the device can be used in measuring the shape of 3D objects. The shape and size of an object can be measured easily by wrapping it with the 3DCS. The human posture can also be measured by wearing it. Second, it is possible to make a soft tactile sensor [7] with the 3DCS by covering compressible materials such as urethane foams with it. If the deformation of the surface of the material is given, the number, shapes, positions of contact objects can be estimated. Furthermore, even the contact force can be measured if the Young's modulus of the material is known. In addition to those applications described above, it is also useful to capture the 3D shapes of clothes for 3D modeling applications.

In this paper, we discuss one of realization methods of the 3DCS. Fig. 1 shows the structure of the 3DCS. A cloth-like sheet has a lattice structure on it. A triaxial accelerometer is attached on each link, and measures the gravity vector. The posture of the link is calculated using the measured gravity. After the postures of all the links are obtained, the whole shape of the sheet is computed by combining the links. A merit of the gravity is that, unlike a magnetic or electric field, the gravity is not disturbed by circumstances. Besides, since our method does not integrate the acceleration to obtain the position, the 3DCS is free from the well-known error accumulation caused by the double integration of the acceleration.

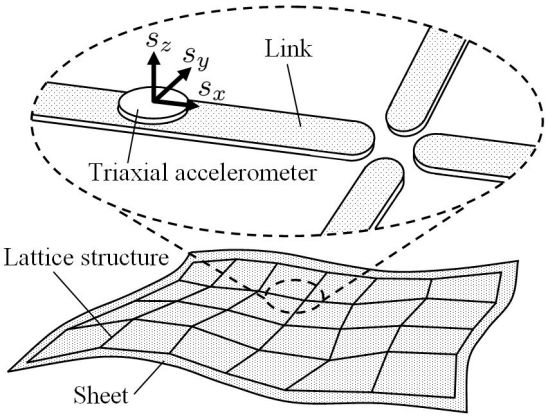

Fig. 1 Illustration of the 3DCS.

The gravity measurement has been used in the motion capture in the preceding reports [9], [10]. They used the gravity to obtain only the roll and pitch angles of a human arm. The output of a single triaxial accelerometer contains only the information about the two angles. Some kinds of assumptions are needed to obtain the yaw angle.

We propose two approaches to obtain the yaw angle. One approach utilizes constraints originating form the lattice structure. The fact that all the links are connected to each other leads two constraints about directional and normal vectors of the links [7], [8]. The other takes the Earth's magnetic field as additional information. It is available everywhere on the Earth as well as the gravity,

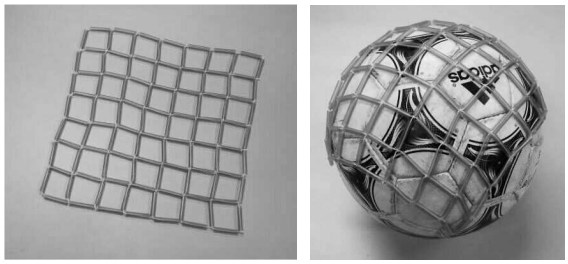

(a) (b)

Fig. 2 (a) Lattice model made of rigid tubes combined with strings (7×7 lattice consisting of 2.5 cm links). (b) The lattice can be mounted on a smooth curved surface. For example, it covers the ball as shown in this figure.

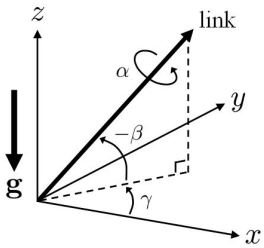

Fig. 3 The gravity vector **g** and the rotational angles. α, β, and γ are the roll, pitch, and yaw angles, respectively. The orthogonal coordinate in this figure means the world coordinate.

and also used in [9], [10] to obtain the orientation.

The following paper outlines first, a description of the basic structure and the problem settings of the 3DCS. Second, the two proposed approaches are explained in Section 3 and 4. Then, Section 5 concludes the paper.

2. 3D CAPTURE SHEET

2.1 Structure

The illustration of the 3DCS is shown in Fig. 1. The 3DCS consists of rigid links forming a lattice structure. A triaxial accelerometer is attached on each link. The accelerometer measures the gravity vector and the measured data are sent to the host computer. The x- and z-axes of the triaxial accelerometer are aligned to be parallel to the direction vector of the link and to the normal vector to the sheet, respectively. The length of each link is the same.

Fig. 2 shows a mock-up of the 3DCS consisting of rigid tubes combined together using strings. Since the length of the link does not change, the lattice structure expands or contracts along the diagonal directions, as is the case with a textile cloth. As shown in Fig. 2 (b), the structure is able to cover a smooth curved surface.

2.2 Problem settings

First, we introduce an assumption to restrict the problem to the static case. The acceleration caused by the motion of the link is negligible compared with the gravity acceleration. The shape estimation in dynamic motion is not considered at least in this stage.

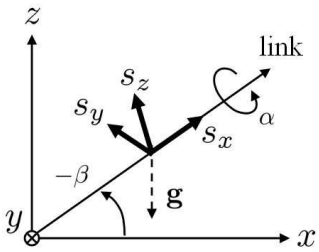

Fig. 4 Side view of the link. The sensor coordinate is rotated according to the roll and pitch angles, α and β.

The 3DCS utilizes the gravity vector **g** (parallel to the z-axis of the world coordinate) measured with the accelerometer attached on each link to estimate its configuration. The posture of each link is described by three angles based on the world coordinate; roll α [rad], pitch β [rad], and yaw γ [rad] (Fig. 3). The roll and pitch angles of each link are calculated from the measured gravity vector, hence the key is how to obtain the yaw angle. The answers to the question are shown in the following sections. After the angles of all the links are obtained, the whole shape of the 3DCS is calculated by combining the links in a computational 3D space.

The angles of the link are obtained as follows. Here we assume that each axis of the triaxial accelerometer is aligned to the corresponding axis of the world coordinate (i.e. the x-axis of the accelerometer to the x-axis of the world coordinate) in the initial condition.

2.3 Derivation of roll and pitch angles

These angles are derived directly from the gravity vector measured with the accelerometer on each link. The rotation matrix $\mathbf{G}_{\beta\alpha}$, from the world coordinate to the sensor coordinate (Fig. 4), is described as

$$\mathbf{G}_{\beta\alpha} \equiv \begin{bmatrix} \cos\beta & 0 & \sin\beta \\ 0 & 1 & 0 \\ -\sin\beta & 0 & \cos\beta \end{bmatrix} \begin{bmatrix} 1 & 0 & 0 \\ 0 & \cos\alpha & -\sin\alpha \\ 0 & \sin\alpha & \cos\alpha \end{bmatrix} = \begin{bmatrix} \cos\beta & \sin\beta\sin\alpha & \sin\beta\cos\alpha \\ 0 & \cos\alpha & -\sin\alpha \\ -\sin\beta & \cos\beta\sin\alpha & \cos\beta\cos\alpha \end{bmatrix}. \quad (1)$$

Each column of $\mathbf{G}_{\beta\alpha}$ means the axis of the sensor coordinate represented in the world coordinate after rotated, and hence the output vector of the accelerometer $\mathbf{a} = [a_x, a_y, a_z]^T$ is represented as a product of the transposed matrix of $\mathbf{G}_{\beta\alpha}$ and the gravity vector $\mathbf{g} = [0, 0, -g]^T$ (where g [m/s^2] is the gravity acceleration);

$$\mathbf{a} = \mathbf{G}_{\beta\alpha}^{T}\,\mathbf{g} = g \begin{bmatrix} \sin\beta \\ -\cos\beta\sin\alpha \\ -\cos\beta\cos\alpha \end{bmatrix}. \quad (2)$$

Then α and β are obtained by solving (2).

3. LATTICE-STRUCTURE APPROACH [8]

3.1 Derivation of yaw angle

This angle cannot be calculated from the output of the single accelerometer. Therefore, in the first approach,

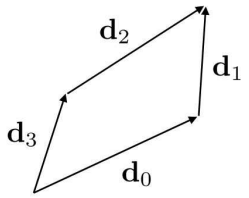

Fig. 5 Assumption 1. Since the lattice unit is a closed loop, the sum of the directional vectors $\mathbf{d}_0$+$\mathbf{d}_1$ is equal to $\mathbf{d}_3$+$\mathbf{d}_2$.

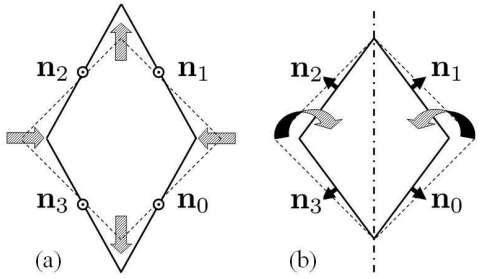

Fig. 6 Assumption 2. We assume two types of symmetric transformations, (a) squashing and (b) folding. In such cases, the sum of the normal vectors $\mathbf{n}_0$+$\mathbf{n}_2$ is equal to $\mathbf{n}_1$+$\mathbf{n}_3$.

we made two assumptions, taking note of one unit of the lattice structure composed of four links forming a quadrangle.

The first assumption is about the directional vector $\mathbf{d}_i$ (i is the link identification) which is represented as

$$\mathbf{d}_i \equiv \begin{bmatrix} \cos\gamma_i & -\sin\gamma_i & 0 \\ \sin\gamma_i & \cos\gamma_i & 0 \\ 0 & 0 & 1 \end{bmatrix} \mathbf{G}_{\beta_i\alpha_i} \begin{bmatrix} 1 \\ 0 \\ 0 \end{bmatrix} = \begin{bmatrix} \cos\gamma_i \cos\beta_i \\ \sin\gamma_i \cos\beta_i \\ -\sin\beta_i \end{bmatrix}. \quad (3)$$

Since the lattice unit is a closed loop (Fig. 5), the two routes reach the same point in the 3D space. That results in the Assumption 1,

[Assumption 1] $\mathbf{d}_0 + \mathbf{d}_1 = \mathbf{d}_3 + \mathbf{d}_2$. (4)

The other assumption is about the normal vector $\mathbf{n}_i$ which is represented as

$$\mathbf{n}_i \equiv \begin{bmatrix} \cos\gamma_i & -\sin\gamma_i & 0 \\ \sin\gamma_i & \cos\gamma_i & 0 \\ 0 & 0 & 1 \end{bmatrix} \mathbf{G}_{\beta_i\alpha_i} \begin{bmatrix} 0 \\ 0 \\ 1 \end{bmatrix}$$
$$= \begin{bmatrix} \cos\gamma_i \sin\beta_i \cos\alpha_i + \sin\gamma_i \sin\alpha_i \\ \sin\gamma_i \sin\beta_i \cos\alpha_i - \cos\gamma_i \sin\alpha_i \\ \cos\beta_i \cos\alpha_i \end{bmatrix}. \quad (5)$$

We assume that the 3DCS is mounted on a smooth curved shape and the lattice unit transforms only in symmetric manners as shown in Fig. 6. In such case, the sum of one pair of the normal vectors of the opposite sides (in Fig. 6, $\mathbf{n}_0$ and $\mathbf{n}_2$, for example) must be equal to that of the other pair ($\mathbf{n}_1$ and $\mathbf{n}_3$). Hence,

[Assumption 2] $\mathbf{n}_0 + \mathbf{n}_2 = \mathbf{n}_1 + \mathbf{n}_3$. (6)

γ_i are obtained by solving (4) and (6). Note that at least one of γ_i should be fixed to a certain value or given because this problem is underdetermined for all the four parameters γ_i in principle. Therefore the obtained yaw angels are relative solutions.

Estimating the configuration of the multi-unit lattice structure is straightforward. After the same algorithm is applied to each lattice unit to obtain the roll, pitch and yaw angles, the whole configuration is estimated by combining the estimated unit shapes.

It is confirmed in [8] that most of the unsolvable conditions are roughly included in the following two cases:

1) All the links of the lattice unit are laid on a horizontal plane.
2) The lattice unit is fully squashed.

Note that Case 2) is avoidable by setting limits to the range of angles of the link joints. Consequently, the essential unsolvable condition is only Case 1).

3.2 Simulation

The purpose of this simulation was to confirm if it was feasible to reconstruct the shape of computational objects based on the proposed algorithm. A computational model of a 13×13 lattice structure comprised of links was used as the model of 3DCS. In this lattice model, the links were modeled as a rigid body so that the length of the link did not change, and the nodes were modeled as a free-joint.

The lattice model was laid over a target computational shape and the position and posture of each link was determined by iterative calculation. According to the calculated postures of the links, the acceleration vectors which were equivalent to the outputs of the accelerometer were acquired.

After that, based on the acquired acceleration vectors, the shape of the computational object was estimated. The roll and pitch angles were analytically determined using (2). In order to obtain the yaw angles using (4) and (6), the following numerical calculation was conducted.

First, we modify (4) and (6) into a minimization problem, that is

$$P \equiv \sum_{j\in\{x,y,z\}} \{(d_{0j} + d_{1j} - d_{2j} - d_{3j})^2 + (n_{0j} - n_{1j} + n_{2j} - n_{3j})^2\} \to \min. \quad (7)$$

where j is the coordinate identification. Here, γ_i are unknown parameters. If the minimum value of P is equal to zero, the solutions for (7) are also the solutions for (4) and (6). Second, we solve (7) by the steepest descent method. Although (7) has several local minima, it is possible to avoid them in most cases by trying multiple initial parameter values.

An example of general situations using a Gaussian as a target shape is shown. Fig. 7 shows the computed lattice model laid over the Gaussian shape (plots at far side) and the reconstructed shape using the acceleration data (plots at near side). The Gaussian shape is successfully reproduced.

3.3 Effect of noise

The results in Fig. 7 were obtained without considering the effects of noise. There are several possible causes of disturbance, including the noise on

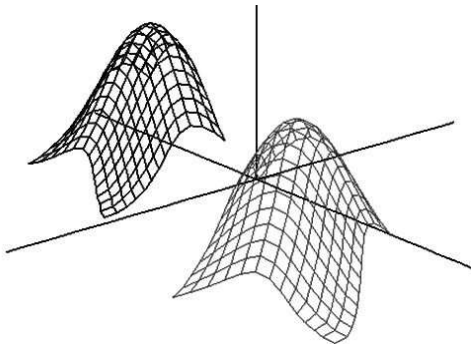

Fig. 7 Simulation results for a Gaussian shape. The far and near plots are the lattice model and the reconstructed shape, respectively.

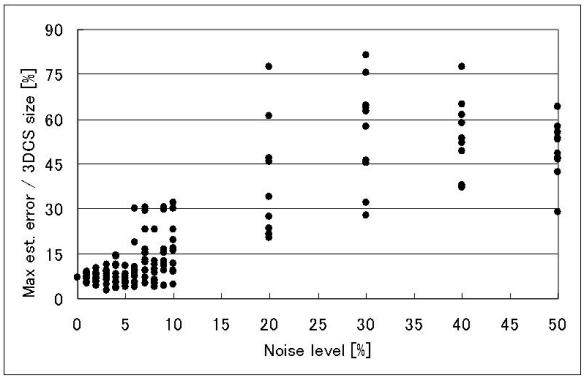

Fig. 8 Simulation results on effect of noise. The maximum values of the estimation error are plotted (10 trials per each noise level).

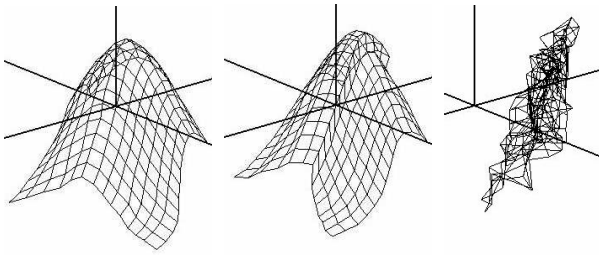

(a) (b) (c)

Fig. 9 Examples of the reconstructed shapes in the cases of (a) 5 %, (b) 6 %, and (c) 50 % noises.

the acceleration data, the change of the link length, and the violation of the Assumption 3 represented as (6). Among the causes listed above, the most major cause is considered to be the noise on the acceleration data. In order to investigate the stability of the 3DCS under various S/N ratios, the following simulation was carried out.

The simulation was carried out in the same manner as described in Section 3.2, except that the noise was added to each component of the acceleration data. The noise was generated using the Mersenne Twister algorithm [11]. The noise level was represented as the percentage of the noise compared to the gravity g.

Fig. 8 shows the maximum values of the estimation errors; the maximum distance between the nodes of the lattice model and the corresponding nodes of the

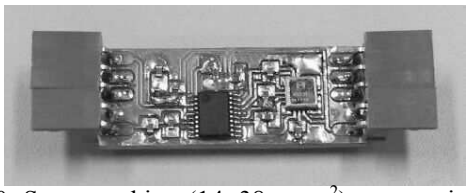

Fig. 10 Sensor chip (14×38 mm^2) measuring the gravity vector and transmitting the measured data to the host PC via an I^2C bus line.

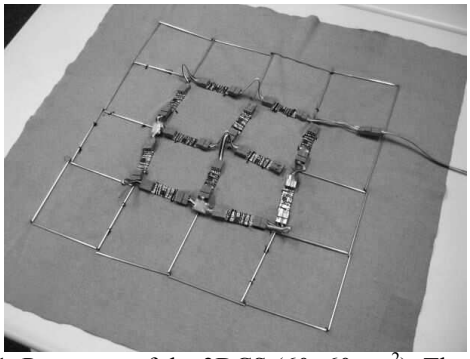

Fig. 11 Prototype of the 3DCS (60×60 cm^2). The length of each link is 10 cm. 12 sensor chips are embedded.

reconstructed model. The estimation errors are normalized by the length of the side of the 3DCS. The reconstructed shape has uncertainty in the absolute position and posture. Therefore, the estimation errors were determined as follows. The sum of the distance between the nodes of the lattice model and the corresponding nodes of the reconstructed model (i.e. the estimation error sum) was calculated. The absolute position and posture of the reconstructed model were varied so that the estimation error sum was minimized based on the least-square method. Note that if no errors are added to the acceleration outputs, the lattice model and the reconstructed shape should be identical. 10 trials per each noise level were conducted. The maximum value of the estimation error among all the nodes was chosen and plotted in Fig. 8 for each trial.

From our observation, it turned out that the 3DCS works under the condition that the noise level is up to 5 % (i.e. about 0.5 m/s^2 in acceleration). It is possible to achieve this noise level when the actual 3DCS is fabricated. A critical estimation error such as Fig. 9 (b) or (c) occurred when the noise level was higher than 6 %.

3.4 Implementation

The integrated sensor chip was developed (Fig. 10). It consists of a triaxial accelerometer (AGS61231, Matsushita Electric Works, Ltd.) and a microcomputer (R8C/16, Renesas Technology Corp.). The analog outputs of the accelerometer are measured by the microcomputer using its 10-bit A/D converter. The microcomputer also transmits the measured data to the host PC via an I^2C bus line.

Fig. 11 shows the prototype of the 3DCS. The side length of the sheet and each link are 60 cm and 10 cm,

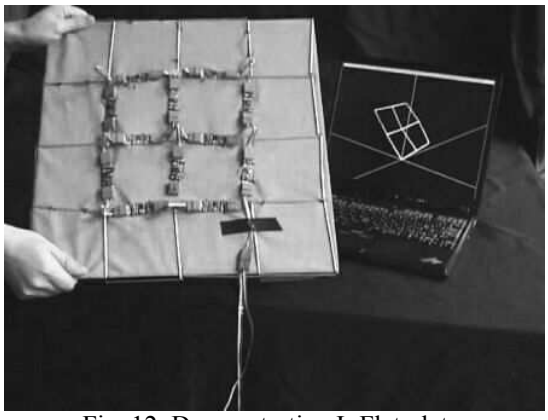

Fig. 12 Demonstration I: Flat plate.

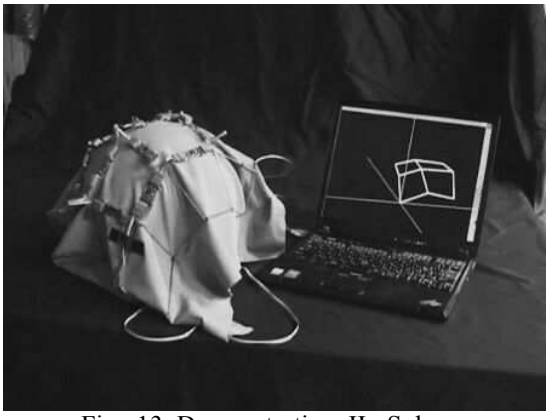

Fig. 13 Demonstration II: Sphere.

respectively. There are 12 sensor chips on the center, and they form a 2×2 lattice structure. The effective sampling rate of the system is 58 Hz. The conjugate gradient method [12] is applied in the estimation process for real-time performance.

Fig. 12 shows the shape estimation of a flat plate. The 2×2 lattice structure was successfully reconstructed in real-time. The slope error of the plate was 4.5 deg and the position error of the nodes is 7 % (i.e. 14 mm in length for 20-cm side length). These errors were caused by the alignment error of the accelerometer, the characteristics of the joint, and the computational error in the estimation process.

Fig. 13 shows the shape estimation of a sphere (23.2 cm in diameter). The lattice structure is also estimated successfully in this case.

4. GEOMAGNETIC APPROACH

4.1 Derivation of yaw angle

The second approach adopts the geomagnetic field in addition to the gravity. The change of the device is only mounting a triaxial magnetometer on each link additionally. All the axes of the magnetometer are aligned to be parallel to the corresponding axes of the accelerometer.

We suppose the Earth's magnetic vector $\mathbf{m}_e$ is perpendicular to the gravity vector $\mathbf{g}$ and parallel to the x-axis (Fig. 14). Then the output of the magnetometer

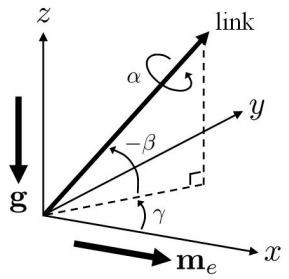

Fig. 14 The gravity and geomagnetic vectors.

$\mathbf{m} = [m_x, m_y, m_z]^{\mathrm{T}}$ is represented as a product of the transposed matrix of $\mathbf{G}_{\gamma\beta\alpha}$ and the geomagnetic vector $\mathbf{m}_e = [m_e, 0, 0]^{\mathrm{T}}$ (where m_e [T] is the Earth magnetism);

$$\mathbf{m} = \mathbf{G}_{\gamma\beta\alpha}^{\mathrm{T}}\,\mathbf{m}_e = m_e \begin{bmatrix} \cos\gamma\sin\beta \\ \cos\gamma\sin\beta\sin\alpha - \sin\gamma\cos\alpha \\ \cos\gamma\sin\beta\cos\alpha + \sin\gamma\sin\alpha \end{bmatrix}, \tag{8}$$

$$\mathbf{G}_{\gamma\beta\alpha} \equiv \begin{bmatrix} \cos\gamma & -\sin\gamma & 0 \\ \sin\gamma & \cos\gamma & 0 \\ 0 & 0 & 1 \end{bmatrix} \mathbf{G}_{\beta\alpha}. \tag{9}$$

Then γ is obtained by solving (8).

Note that the geomagnetic vector is not horizontal precisely, and the magnetometer output **m** is not perpendicular to the accelerometer output **a**. Hence we use the perpendicular component **m**' that is calculated as

$$\mathbf{m}' = \mathbf{m} - \left(\mathbf{m} \cdot \frac{\mathbf{a}}{|\mathbf{a}|}\right)\frac{\mathbf{a}}{|\mathbf{a}|}. \tag{10}$$

The yaw angle can be obtained unless $\mathbf{m}' = \mathbf{0}$.

Estimating the configuration of the whole shape is as follows. After the same algorithm is applied to each link to obtain the roll, pitch and yaw angles, the whole configuration is estimated by combining them.

In this procedure, a compensation of yaw angles can be applied. The geomagnetic field is easily disturbed by magnet sources such as magnets or coils. Then the magnetic vectors at the sensor positions are no longer parallel, and estimated links do not make closed loop. In fact, this error is compensable by solving (4) about γ_i around the estimated values. The algorithm proposed above is, as a result, undisturbed by the magnet sources being located at a certain distance from the surface of the sheet.

4.2 Effect of noise

In order to investigate the stability of the 3DCS under various S/N ratios, a simulation was carried out in the same manner as described in Section 3.3, except that the noise was added also to each component of the magnetic data. The noise level of the magnetic data was represented as the percentage of the noise compared to the horizontal geomagnetic field m_e.

Fig. 15 shows the maximum values of the estimation errors as the function of the acceleration and magnetic noise levels. It can be said from Fig. 8 that the maximum estimation error higher than 15 % is critical. Based on that benchmark, it turns out that the noise level is allowed up to 8 % for acceleration data and 25 % for magnetic data.

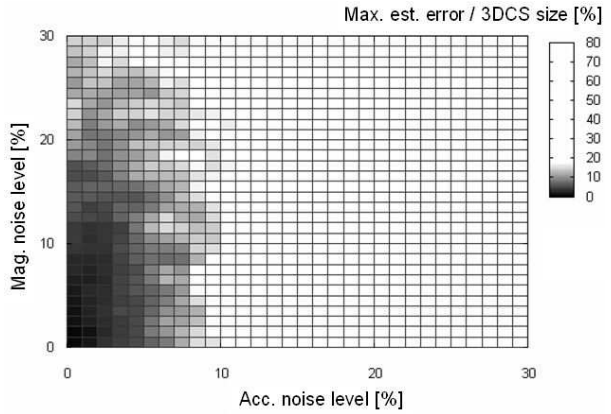

Fig. 15 Simulation results on effect of noise. The worst cases of the maximum estimation error, i.e. the envelope of the error plot, are shown (10 trials per each noise level). The area where the maximum estimation error is lower than 15 % is colored deeply.

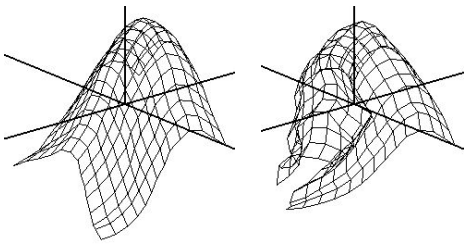

(a) (b)

Fig. 16 Examples in the cases of (a) 5 % acc. and 20 % mag. noises, and (b) 10 % acc. and 20 % mag. noises.

4.3 Implementation

We are in the process of developing a prototype of the gravity- and geomagnetic-based 3DCS. A small-sized sensor chip which consists of a 3-axis accelerometer and a 3-axis magnetometer will be fabricated.

5. CONCLUSION

This paper proposed a new flexible sensing device "3DCS," which measures its own 3D configuration using distributed triaxial accelerometers. The details of the structure and two approaches of the shape estimation algorithm are described. Their feasibility is verified by simulation. The 2×2 prototype based on the first approach succeeded in estimating the shapes of a flat plate and a sphere with 7 % estimation error. Development of the prototype based on the second approach is in progress.

In the future, we will develop a small-sized sensor chip on which a customized LSI is mounted with a triaxial accelerometer (and a magnetometer). The LSI is designed to receive the sensor readouts and send digital data to the host computer via the two-dimensional communication sheet [5]. The required electrical power is also supplied via the same sheet to the sensor chips. Combining together with these technologies, the practical 3DCS will be realized without complicated long signal/power wires.

REFERENCES

[1] E. R. Post and M. Orth, " Smart fabric, or "wearable clothing"," *Proc. 1st IEEE International Symposium on Wearable Computers (ISWC '97)*, pp. 167-168, 1997.

[2] J. Farringdon, A. J. Moore, N. Tilbury, J. Church, and P. D. Biemond, "Wearable sensor badge and sensor jacket for context awareness," *Proc. 3rd IEEE International Symposium on Wearable Computers (ISWC '99)*, pp. 107-113, 1999.

[3] T. Linz, C. Kallmayer, R. Aschenbrenner, and H. Reichel, " Embroidering electrical interconnects with conductive yarn for the integration of flexible electronic modules into fabric," *Proc. 9th IEEE International Symposium on Wearable Computers (ISWC '05)*, pp. 86-91, 2005.

[4] O. Brand, " Microsensor Integration into Systems-on-Chip," *Proc. IEEE*, vol. 94, no. 6, pp. 1160-1176, 2006.

[5] Y. Makino, H. Chigusa and H. Shinoda, "Two-dimensional sensor integration using resonant proximity connector -Basic technology and application to elastic interface device-," P*roc. 3rd International Conference on Networked Sensing Systems (INSS 2006)*, pp. 196-202, 2006.

[6] M. Petrov, A. Talapov, T. Robertson, A. Lebedev, A. Zhilyaev, and L. Polonskiy, "Optical 3D digitizers: Bringing life to the virtual world," *IEEE Computer Graphics and Applications*, vol. 18, pp. 28-37, 1998.

[7] T. Hoshi and H. Shinoda, "Free-form tactile sensor using 3-dimensional shape capture sheet," *Proc. 2nd Joint Eurohaptics Conference and Symposium on Haptic Interfaces for Virtual Environment and Teleoperator Systems (World Haptics 2007)*, pp. 403-408, 2007.

[8] T. Hoshi, S. Ozaki, and H. Shinoda, "Three-Dimensional Shape Capture Sheet Using Distributed Triaxial Accelerometers," *Proc. 4th International Conference on Networked Sensing Systems (INSS 2007)*, pp. 207-212, 2007.

[9] J. Lee and I. Ha, "Real-time motion capture for a human body using accelerometers," *Robotica*, vol. 19, pp. 601-610, 2001.

[10] N. Miller, O. C. Jenkins, M. Kallmann, and M. J. Mataric, "Motion capture from inertial sensing for untethered humanoid teleoperation," *Proc. 4th IEEE/RAS International Conference on Humanoid Robots (Humanoids 2004)*, vol. 2, pp. 547-565, 2004.

[11] M. Matsumoto and T. Nishimura, " Mersenne Twister: A 623-dimensionally equidistributed uniform pseudorandom number generator," *ACM Trans. on Modeling and Computer Simulation*, vol. 8, no. 1, pp.3-30, 1998.

[12] W. H. Press, S. A. Teukolsky, W. T. Vetterling, and B. P. Flannery, *Numerical Recipes in C: The Art of Scientific Computing Second Edition*, Cambridge University Press, 1992.